Report of Test

Absolute Spectral Radiance Responsivity

of the

NASA GLAMR Si Radiometer
Model LTD-11, S/N 104

Request Submitted by:

Joel McCorkle
NASA Goddard Space Flight Center
Greenbelt, MD

1. Description of Calibration Items

The device under test (DUT) is a silicon radiance meter manufactured by L-1 Standards and Technology, Inc. (L-1), model LTD-11, S/N 104 and referred to as GLAMR Si. The device is housed in a 2-inch diameter tube with a fore-optic consisting of an aperture and lens. The detector is temperature controlled (L-1 model 3100-1L, S/N 12105) at 29.0 °C and the rear of the device has inputs for the L-1 temperature controller and a BNC output for the detector signal. The detector came with an L-1 model 3300v2, S/N 027, transimpedance amplifier which was used for the calibration. Figure 1.1 shows the detector and accessory equipment as received.

Figure 1.1 Picture of GLAMR Si Radiometer as received, where it was packaged together with the GLAMR InGaAs Radiometer. The leftmost picture shows the radiometer and the box containing the transimpedance amplifier. Front (middle) and back (right) views of the temperature controller are also shown.

1.1 Calibration Request

The request was to calibrate the DUT for absolute radiance responsivity from 320 nm to 400 nm with a standard uncertainty of 0.5 % (k=1) or better and from 400 nm to 885 nm with a standard uncertainty of 0.06 % (k=1) or better.

2. Description of Test

The detector was characterized for absolute spectral radiance responsivity on the NIST facility for Spectral Irradiance and Radiance responsivity Calibrations using Uniform Sources (SIRCUS).[1,2] The calibration took place in various stages from Aug. 07, 2019 to Sept. 18, 2019. During each calibration test, the detector was temperature controlled at 29.0 °C by the L-1 controller and checked at the beginning and end of each calibration session.

This calibration was performed in two parts. First, the spectral range 380 nm to 900 nm was completed using T-01 as the standard reference detector. Second, the spectral range 347 nm to 450 nm was completed using an ultraviolet (UV) enhanced detector, IRD WS #2, as the standard reference detector. For this part, an irradiance calibration of IRD WS #2 was also necessary. Using a power responsivity scale completed from 300 nm to 400 nm previously[3] and an irradiance scale transfer from T-01 from 380 nm to 450 nm, an irradiance scale was generated for IRD WS #2 from 300 nm to 450 nm. This scale transfer was completed simultaneously with the GLAMR Si Calibration.

Description of laser systems used: Several laser systems were used to cover the specified ranges for the various parts of the calibration.

1. A Picosecond mode-locked lithium triborate-optical parametric oscillator (LBO-OPO) laser (~80 mHz repetition rate) was used that consists of two separate cavities. The main cavity is designed to oscillate the signal beam and the other cavity is designed to intracavity double the oscillated idler beam.
   a. The signal output of the main cavity was used between 765 nm and 910 nm.
   b. The signal output from the main cavity was doubled in a beta-barium borate (BBO) crystal (second harmonic generation, SHG) and used from 380 nm to 530 nm.
   c. The output of the intracavity doubled laser was used from 540 nm to 610 nm.
2. A Ti:Sapphire laser (Continuous Wave, CW) was used in two ranges
   a. Using the DCM output coupler from 700 nm to 720 nm.
   b. Using the Short-Wave output coupler from 705 to 746 nm.
3. A 4-(Dicyanomethylene)-2-methyl-6-(4-dimethylaminostyryl)-4*H*-pyran (DCM) dye laser (CW, Coherent CR699) was used from 635 nm to 670 nm.
4. A femtosecond (~ 100 fs pulse width) mode-locked Ti:Sapphire laser (Spectra Physics Mai Tai) was used from 690 nm to 746 nm.
5. The Mai Tai laser was also coupled into a Spectra Physics Inspire HF 100 laser and the SHG output was used from 347 nm to 450 nm. This was used primarily for the calibration with IRD WS #2 as the standard reference detector.

The output from lasers was coupled to an optical fiber. The optical fiber was in turn connected to a side port on the integrating sphere and illuminated an area toward the front of the sphere. For the DCM dye laser and the Ti:sapphire laser, a section of fiber was placed into an ultrasonic bath to reduce effects due to laser speckle. For the LBO-OPO and Mai Tai systems, the ultrasonic bath was not required. For each laser, a Brokton Electro-Optics Corporation (BEOC) laser power controller stabilized the beam to less than the 0.1 % level using feedback from a photodiode in the sphere, removing short term as well as long term fluctuations in the power output from the various laser sources. A Coherent WaveMaster (S/N: W0385) measured the wavelength for the DCM dye

laser and Ti:Sapphire laser, while a Bristol 621 wavemeter (S/N: 6208) was used for the LBO-OPO system. For the Mai Tai system, a portion of the beam was directed to an integrating sphere and the wavelength was measured with an Ocean Optics, Inc. JAZ spectrometer (S/N: JAZA0657) that has been calibrated to a mercury pen lamp. All wavelengths were converted to the air value for data analysis by dividing by a factor of 1.00027. In the case of the externally doubled LBO-OPO, the signal wavelength was measured directly and the actual wavelength value, WL, was determined as WL = (measured WL)/2. In the case of the intracavity doubled LBO-OPO, the signal wavelength was measured directly, and the actual wavelength was determined according to equation 2.1,

$$\lambda = \frac{1}{2\left(\frac{1}{\lambda_{pump}} - \frac{1}{\lambda_{signal}}\right)} \qquad (2.1)$$

where λ_{pump} is 532.2 nm, λ_{signal} is measured by the Bristol wavemeter, and the factor of two converts to the second harmonic of the idler.

Integrating Sphere: The integrating sphere used for radiance responsivity was a LabSphere 30.48 cm (12") diameter, Spectralon-coated sphere equipped with a 5.08 cm (2") diameter exit aperture fabricated by LabSphere (non-point source geometry).

Data Acquisition and Control Program: The data was acquired using the SIRCUS Main Program v10. Background subtracted DC signals were sequentially collected for each detector (DUT and reference standard) along with simultaneously recorded monitor signals (also background subtracted). The collections were repeated 11 times. Each repeat sample was ratioed to the monitor signal and the average and percent standard deviation was determined.

Description of calibration detectors: The working standard reference trap detector T-01 was used to measure the radiance and irradiance emitted from the source sphere from 380 nm to 910 nm. It was equipped with an aperture having an area of 19.6591 mm^2 and a precision transimpedance amplifier, Prec#2, was used with the trap detector. T-01 was previously calibrated for irradiance responsivity with scales traceable to the NIST Primary Optical Watt Radiometer (POWR).[4] The responsivity scale for T-01 is derived from a SIRCUS calibration using T-06 as the reference standard detector,[5] where T-06 was calibrated directly against POWR.[6,7]

The monitor detector was a silicon photodiode mounted directly to the source sphere.

The standard reference detector for the UV range was IRD WS #2 and was used to determine the radiance of the source from 347 nm to 450 nm. It was equipped with an aperture having an area of 9.660 mm^2, as determined radiometrically, and connected to a transimpedance amplifier (L-1 model 3300v2, S/N: 3300v2-016).

3-axis stage: The integrating sphere is mounted on an XYZ translation stage, with the Z-position (along the optical axis) measured with a linear encoder. The X- and Y-axes enable the source to be properly positioned in front of an instrument before it measures the sphere radiance. The Z-position is used to accurately determine the separation between relevant apertures.

Measurement Setup: Detectors used in these experiments were mounted to tip-tilt stages and aligned to the optical axis of the integrating sphere source using a double-headed laser. To align the detectors to the sphere, the double-headed laser was first mounted in-front of the large sphere

where one end of the laser was previously aligned to the center of the sphere aperture. The other end of the laser was retroreflected from a glass microscope slide on each detector to align to the optical axis. Lastly, the laser was centered on each detector using the 3-axis stage to determine the X,Y position. See Figures 2.1 and 2.2 for photographs of the measurement setup and Figure 2.3 for a photograph of the temperature controller setup.

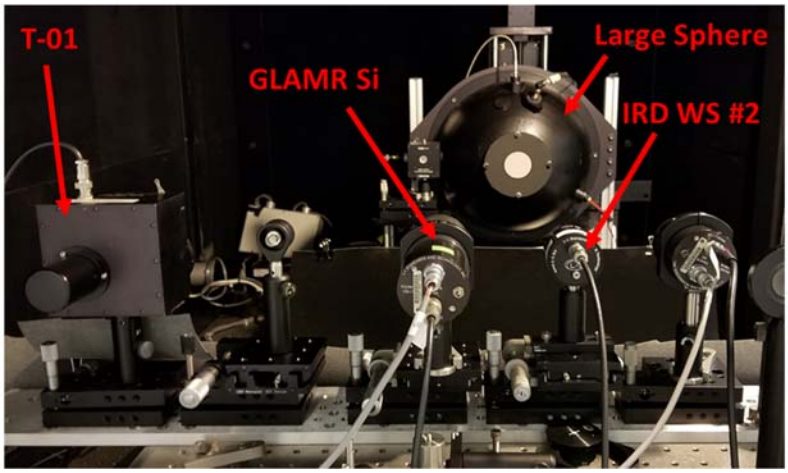

Figure 2.1 Back-view of detector bench setup for the radiance measurements of the DUT using both T-01 and IRD WS #2 as the standard reference detectors.

Figure 2.2 Side-view of detector bench setup for radiance measurements of the DUT using both T-01 and IRD WS #2 as the standard reference detectors.

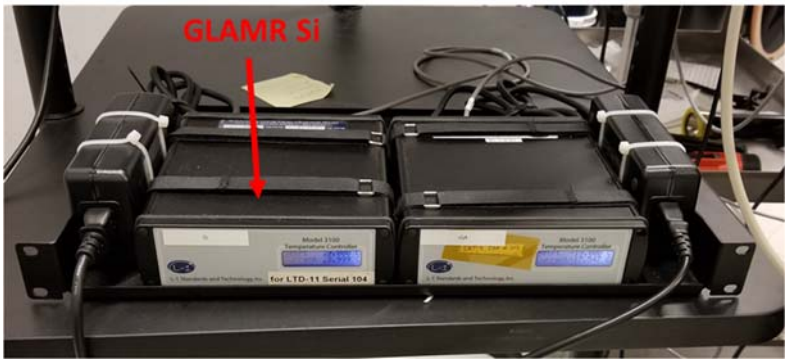

Figure 2.3 Photograph showing the setup of the temperature controllers

2.1 Irradiance Responsivity Scale Transfer from T-01 to IRD WS #2

An irradiance measurement was performed to transfer the irradiance responsivity scale from T-01 to IRD WS #2. Irradiance measurements were collected from 380 nm to 450 nm and combined with power responsivity measurements from 300 nm to 400 nm. The power responsivity curve was scaled using tie points at 380 nm, 390 nm, and 400 nm by a scaling factor determined as the ratio of the irradiance to power responsivity at these points. The irradiance responsivity scale for IRD WS #2 therefore consists of the scaled power responsivity from 300 nm to 400 nm and the measured irradiance responsivity from T-01 for 400 nm to 450 nm. All measurements for this part were done with the sphere at z = -91.953 mm. The detector positions were determined radiometrically as described in Section 3.2, below, and yield the working distance along with the known Z-position.

The pre-amplifier gain was 1 x 10^7 V/A for both detectors for all measurements.

2.2 Radiance Responsivity of GLAMR Si from IRD WS #2

Absolute radiance responsivity measurements for GLAMR Si (with associated transimpedance amplifier) versus the UV protected reference standard detector, IRD WS #2, were completed at discrete wavelengths between 347 nm to 450 nm using the SIRCUS facility. The integrating sphere source was the 12” diameter sphere described in Section 2 with a 5.08 cm (2”) aperture.

The sphere was moved between different positions for GLAMR Si and reference standard detector measurements. For GLAMR Si, a Z-position of - 525.85 mm was used. This Z-position was approximately 28 cm away from the front aperture of the DUT, which placed the field of view completely within the 2-inch diameter sphere output aperture. An X-Y response map for the DUT was also measured, verifying the central position and underfilled configuration of the DUT relative to the sphere aperture. The sphere was placed at a different Z-position, -91.953 mm, for measurements of the sphere radiance with IRD WS #2. This placed the sphere aperture well within the acceptance angle of the working reference detector for power measurement as suggested in Section 3.1, below. The working distance for IRD WS #2 was determined from the sphere Z-position and the radiometrically determined detector position, as described in Section 3.2 below.

The pre-amplifier gain was 1 x 10^7 V/A for both detectors for all measurements.

2.3 Radiance Responsivity of GLAMR Si from T-01

Absolute radiance responsivity measurements for GLAMR Si (with associated transimpedance amplifier) versus the NIST tunnel trap detector, T-01, were completed at discrete wavelengths between 380 nm to 915 nm using the SIRCUS facility. This was done similarly as described in Section 2.2, above, except the Z-position for the sphere radiance measurement by T-01 was -103.40 mm. The working distance for T-01 was also determined from the sphere Z-position and the radiometrically determined detector position, as described in Section 3.2 below. At the working distance, the sphere aperture was well within the acceptance angle of the working reference detector for power measurement as suggested in Section 3.1, below.

The pre-amplifier gain was 1 x 10^7 V/A for both detectors for nearly all measurements except for 510 nm to 530 nm where the pre-amplifier gain was 1 x 10^8 V/A.

3. Results of Test

For this calibration, both an irradiance and a radiance measurement were performed. In both cases, the reference detector (trap T-01 or IRD WS #2) establishes the irradiance at the detector aperture plane or the radiance emitted from the source sphere. Even though the reference detectors are irradiance meters, they are also used to determine the source radiance, requiring knowledge of the solid angle of the source. To determine the solid angle, the distance between the trap aperture and the integrating sphere source aperture was measured, along with the integrating sphere and trap aperture areas: See Section 3.1. For the irradiance measurements, the irradiance of the source must be known at the test detector (IRD WS #2) reference plane. This is done by applying a correction factor to the measured source irradiance at the reference detector reference plane that is derived from the relative positions of the two detectors. The detector positions are determined radiometrically, as described in Section 3.2, and the distance of each from the source is determined by measuring the Z-position with the linear encoder on the Z-axis stage.

3.1 Determination of the sphere source radiance

The radiance of the sphere source was determined with the flux transfer method. A working reference detector (T-01 or IRD WS #2) measured the radiant power from the sphere source passing through two precision apertures, one on the source side, another on the detector side.

The radiance L [W m^{-2} sr^{-1}] of the sphere was determined from radiant power P [W] and the geometric extent G by:

$$L = \frac{P}{G} \tag{3.1}$$

The geometric extent G [m^2 sr] is given by

$$G = \frac{\pi^2}{2}\left[(d^2 + r_s^2 + r_D^2) - \{(d^2 + r_s^2 + r_D^2)^2 - 4r_s^2 r_D^2\}^{1/2}\right] \tag{3.2}$$

where r_S is the radius of the aperture in front of the source, r_D is the radius of the aperture in front of the detector, and d is the distance between the two apertures. The diameter of the sphere aperture was large enough (50.8 mm) to overfill the radiance measurement angle of the DUT radiometer by the sphere output radiation. The distance, d, was chosen large enough (~ 725.00 mm for T-01 and ~ 730 mm for IRD WS #2) so that the sphere aperture was well within the acceptance angle of the working reference detector for power measurement.

3.2 Detector offset and offset uncertainty determination for irradiance meters

For both radiance and irradiance measurements, knowledge of a distance between the source and a detector aperture is required. For the irradiance measurements in the scale transfer step of Section 2.1, the distance for both T-01 (the working reference) and IRD WS #2 (the test detector) was determined. For the radiance measurement, only the distance for the working reference detectors was determined. All distances were determined radiometrically.

In general, at several different Z positions, the detector and monitor voltages were recorded to yield a relative irradiance. Using the $1/Z^2$ law for on-axis irradiance (inverse square law) the resultant data can be fit by a point-source geometry (Equation 3.3) and a non-point-source geometry (the experimental configuration, Equation 3.4) to yield the Z-position of the detector aperture plane. From the Z-position encoder reading used in the radiance and irradiance measurements and the detector Z-position from the radiometric $1/Z^2$ law fit, the actual detector aperture to sphere aperture distance in millimeters (working distance) was determined. Figure 3.1 is a schematic of the configuration.

The inverse square law fitting equation for a point-source geometry is:

$$y = \frac{m_1}{(M_0 - m_2)^2} \tag{3.3}$$

Where y is the relative irradiance, m_1 is a fitting constant, M_0 is Z-position of the integrating sphere that is read by the Z-encoder, and m_2 is the Z-position of zero offset between the two apertures. The fitting uncertainty in m_2, for the sphere position during calibration, gives the uncertainty in the distance between the two apertures.

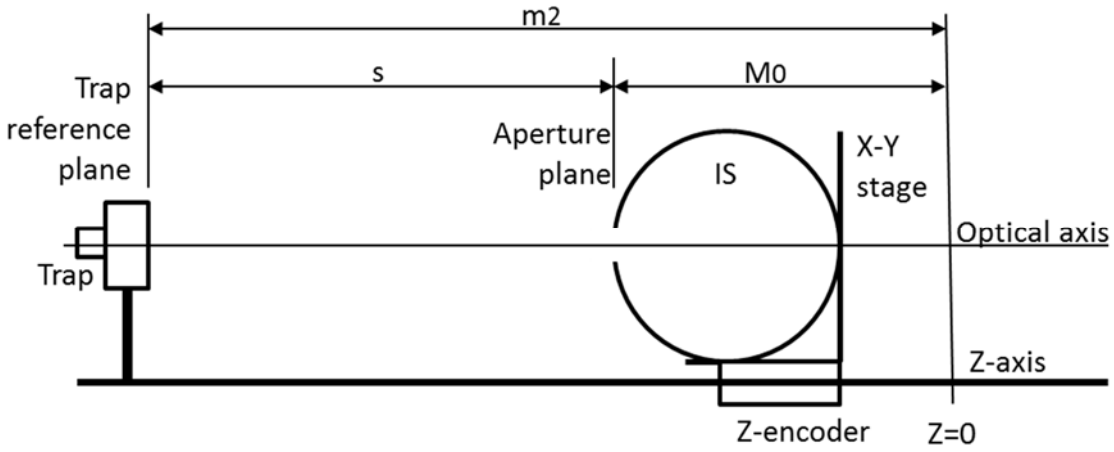

Figure 3.1. Schematic of the configuration for determining trap-sphere distance radiometrically.

If the source aperture is large, the non-point source geometry expression is fit to the data:

$$y = \frac{m_1}{((M_0 - m_2)^2 + m_3^2 + m_4^2)} \tag{3.4}$$

where y, m_1, M_0, and m_2 are the same as in Eq. 3. $m_3 = r_d$, the radius of the detector aperture, and $m_4 = r_s$, the radius of the integrating sphere aperture. Equation 3.4 is valid in the limit where

$$(r_s^2 + r_d^2 + s^2) \gg 2r_s r_d \tag{3.5}$$

and s is the distance between the source and detector apertures. The inverse square law measurements along with the fit of equation 3.4 to the data for each detector can be seen in Figures 3.2 and 3.3, below. At a separation, s, equal to the working distance, the ratio given by equation 3.5 was determined for each detector. This result is summarized in Table 3.1 and shows the condition of equation 3.5 holds and that equation 3.4 is valid in each case. The residuals are approximately 3 orders of magnitude smaller than the base measurement and show there is no obvious bias or offset. The fitting results are also summarized in Table 3.2.

For irradiance measurements, a correction factor (CF) in the source irradiance arises due to slight differences in the working distance between the DUT and reference standard detectors. The correction factor is determined according to equation 3.6 and the detector radius, r_d, refers to either the standard reference detector or the DUT.

$$CF = \frac{r_s^2 + r_{d,ref}^2 + s_{ref}^2}{r_s^2 + r_{d,ref}^2 + s_{DUT}^2} \tag{3.6}$$

Applying this correction factor gives the source irradiance as measured by the reference standard detector at the DUT reference plane.

Table 3.1 Results of equation 3.5 at minimum separation distances.

Detector	r_s (cm)	r_d (cm)	s (cm)	Ratio (Eq 3.5)
IRD WS #2	2.54	0.175	72.9	5985
T-01	2.54	0.25	72.5	4143

Table 3.2 Results of the inverse square law fits of equation 3.4 to the data.

Detector	m_2 (mm)	Fitting Uncertainty (mm) (k=1)	R, fit
IRD WS #2	-821.08	0.156	1
T-01	-816.95	0.0585	1

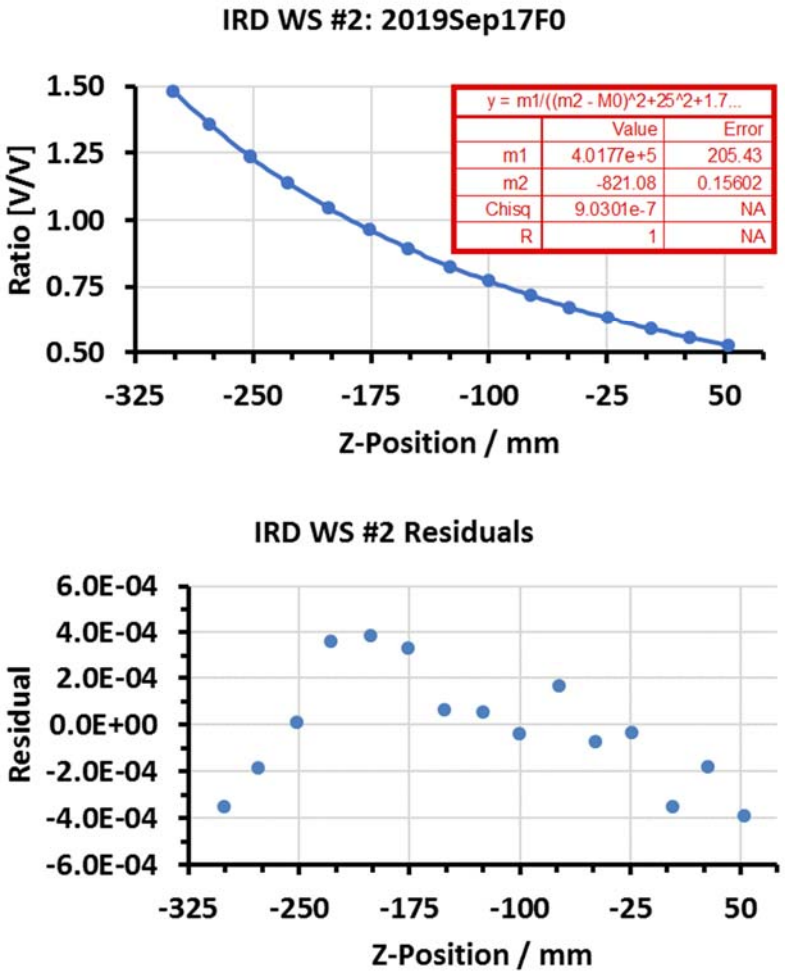

Figure 3.2 Offset and uncertainty fit of the non-point source geometry equation 3.4 to the irradiance response data at a wavelength of 450 nm (top) and residuals from the fit (bottom) for distance determination of IRD WS #2.

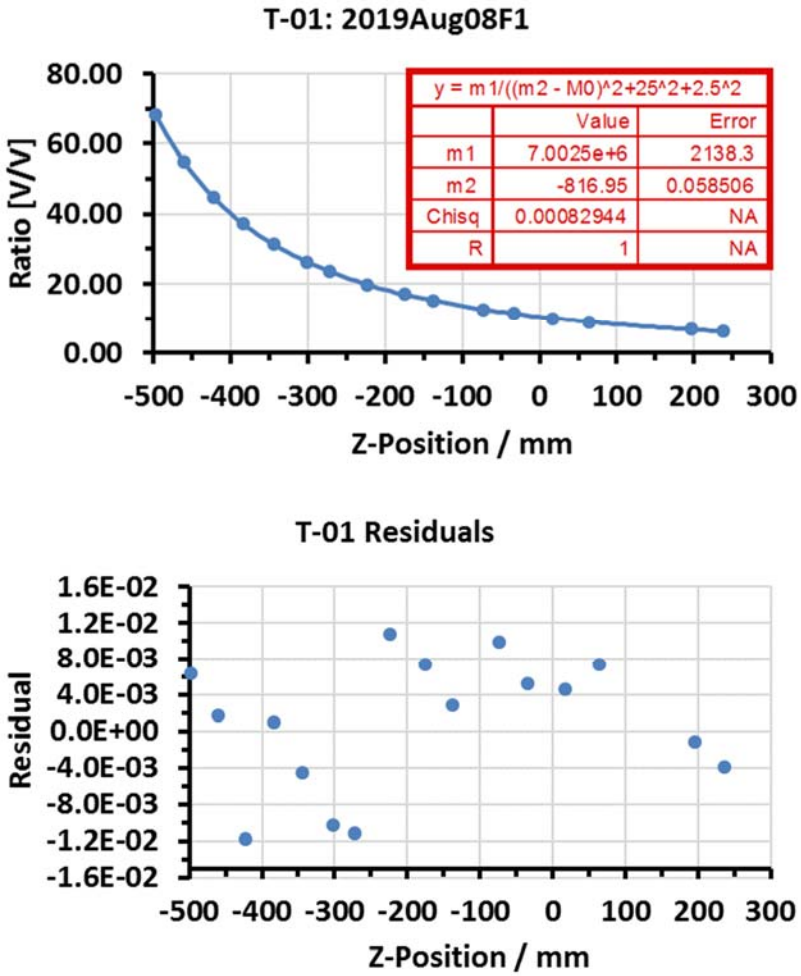

Figure 3.3 Offset and uncertainty fit of the non-point source geometry equation 3.4 to the irradiance response data at a wavelength of 806 nm (top) and residuals from the fit (bottom) for distance determination of T-01.

3.3 Irradiance responsivity of IRD WS #2 from T-01 and Power Responsivity

The irradiance responsivity of IRD WS #2 from 300 nm to 450 nm was determined by a combination of data. First, the irradiance responsivity relative to T-01 was measured from 380 nm to 450 nm. A correction factor of 0.9887 was applied to determine the source irradiance at the IRD WS #2 reference plane due to the slight difference in working distance between T-01 and IRD WS #2. Second, the power responsivity had been previously measured on POWR from 300 nm to 400 nm.[3] The ratio of the irradiance responsivity to power responsivity was determined at three points where the two curves overlap: 400 nm, 390 nm, and 380 nm. A scaling factor of 0.09654 cm^2 was determined as the average ratio at these three points with a percent standard deviation of 0.09 % and used to scale the power responsivity curve to irradiance responsivity values. This yielded the overall responsivity curve as the scaled power responsivity from 300 nm to 400 nm and the irradiance responsivity determined directly from T-01 from 400 nm to 450 nm, which is shown in Figure 3.4.

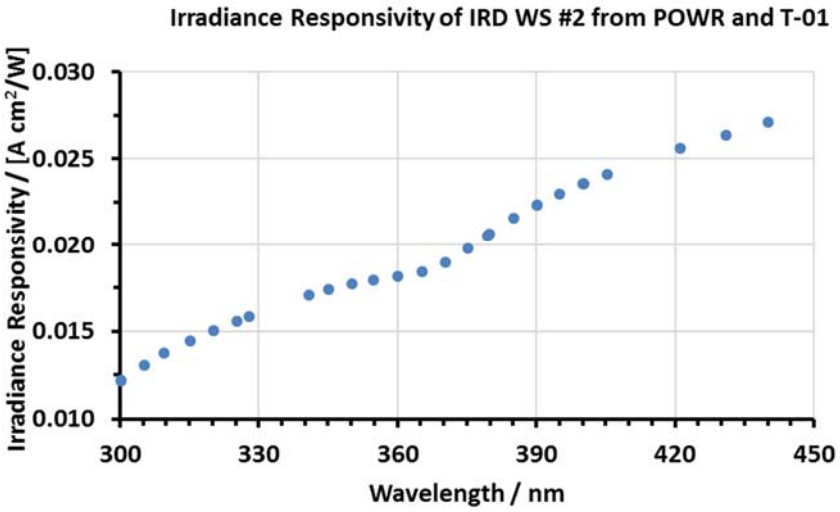

Figure 3.4 Irradiance Responsivity for IRD WS #2 from POWR and T-01.

Table 3.3 Irradiance Responsivity Data for IRD WS #2

Wavelength [nm]	Irradiance Responsivity [A cm²/W)]	% Uncertainty [A cm²/W] (k=1)
300.3	0.01218	0.19
305.3	0.01308	0.19
309.6	0.01373	0.19
315.1	0.01443	0.19
320.2	0.01503	0.19
325.2	0.01557	0.19
328.0	0.01587	0.19
340.8	0.01710	0.19
345.2	0.01744	0.19
350.1	0.01775	0.19
354.9	0.01796	0.19
360.1	0.01815	0.19
365.3	0.01845	0.19
370.3	0.01900	0.19
375.2	0.01978	0.19
379.8	0.02063	0.19
385.2	0.02155	0.19
390.2	0.02231	0.19
395.0	0.02294	0.19
400.0	0.02355	0.19
405.3	0.02411	0.12
421.1	0.02559	0.12

431.1	0.02638	0.12
440.2	0.02710	0.12
450.1	0.02781	0.12

3.4 Uncertainty analysis for the irradiance responsivity scale of IRD WS #2

Table 3.4 Uncertainty Budget for Absolute Spectral Irradiance Responsivity of IRD WS#2.

	Relative Standard Uncertainty [%]	
Uncertainty Component	**300 nm to 400 nm**	**400 nm to 450 nm**
Power Responsivity Calibration	0.1	N.A.
Power Responsivity Scaling Factor	0.1	N.A.
Reference detector Irrad. Cal. (T-01 from T-06)	0.09	0.09
Irradiance Measurement %Standard Deviation[1]	0.032	0.015
Amplifier gain	0.05	0.05
Geometry Alignment	0.05	0.05
Reference Detector Aperture Area	0.02	0.02
Sphere Aperture Area	0.03	0.03
Reference Detector Distance	0.01	0.01
DUT Distance	0.02	0.02
Wavelength	0.03	0.03
Combined Standard Uncertainty (k=1)	**0.19**	**0.12**

Note 1: For 300 nm to 400 nm, this entry is the average % St. Dev. of the measurements at the tie points (380 nm, 390 nm, and 400 nm). For 400 nm to 450 nm, this entry is the average % St. Dev. of the measurements in this range.
Note 2: This is not the full calibration uncertainty budget. The uncertainty budget, Table 3.4, does not include environmental effects on both the reference detector and the GLAMR radiometer. No evaluations of instrument performance characteristics such as temperature dependence, response linearity or temporal stability were performed. For estimates in the interpolated uncertainty, see the reference.[8]

3.6 Radiance Responsivity of GLAMR Si

Radiance responsivity of GLAMR Si was measured from 347 nm to 910 nm using two standard reference detectors to cover the separate but overlapping spectral ranges. Standard reference detector T-01 was used from 380 nm to 910 nm and IRD WS #2 was used from 347 nm to 450 nm as shown in Figure 3.8. In the overlap region 380 nm to 450 nm, good agreement within the standard uncertainties was found between the responsivities derived from the two reference detectors. Comparing the absolute values measured when using IRD WS #2 and T-01 (extrapolated to equivalent wavelengths) resulted in an average percent difference of 0.08 %, where it should be noted that the percent difference for the last two points at 440 nm and 450 nm was notably higher at -0.16 % and -0.24 %, respectively.

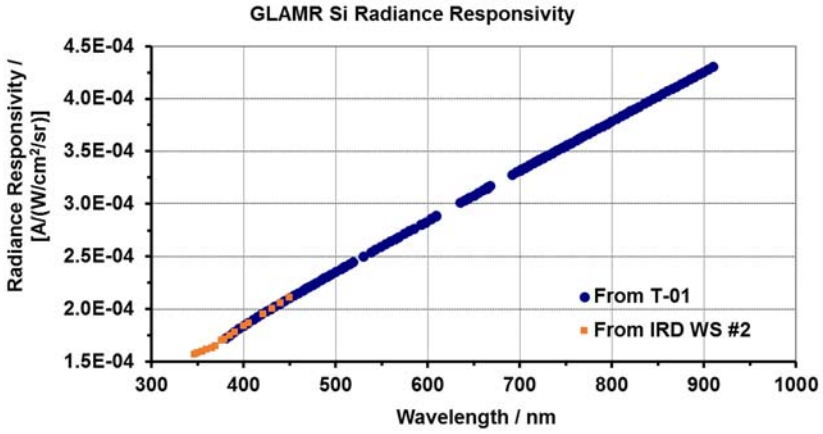

Figure 3.8 Radiance responsivity of GLAMR Si radiometer from T-01 (blue circles) and IRD WS #2 (orange squares).

Table 3.5 Tabulated absolute spectral radiance responsivity data for GLAMR Si.

Reference Detector	Wavelength [nm]	Radiance Responsivity [A/(W/cm²/sr)]	% Uncertainty (k=1)
IRD WS #2	347.00	1.567E-04	0.27
IRD WS #2	350.15	1.580E-04	0.21
IRD WS #2	355.03	1.596E-04	0.21
IRD WS #2	360.00	1.612E-04	0.21
IRD WS #2	365.33	1.630E-04	0.21
IRD WS #2	369.60	1.650E-04	0.21
IRD WS #2	376.02	1.697E-04	0.21
IRD WS #2	377.51	1.698E-04	0.21
IRD WS #2	379.54	1.712E-04	0.22
T-01	380.89	1.722E-04	0.12
T-01	385.09	1.750E-04	0.12
IRD WS #2	385.22	1.749E-04	0.21
T-01	389.95	1.780E-04	0.12
IRD WS #2	390.25	1.781E-04	0.21

T-01	395.14	1.810E-04	0.12
IRD WS #2	400.21	1.840E-04	0.21
T-01	400.26	1.840E-04	0.12
T-01	404.70	1.866E-04	0.12
T-01	404.91	1.866E-04	0.12
IRD WS #2	405.26	1.868E-04	0.15
T-01	410.72	1.898E-04	0.12
T-01	415.62	1.924E-04	0.13
T-01	420.19	1.949E-04	0.13
IRD WS #2	421.09	1.955E-04	0.15
T-01	425.10	1.975E-04	0.12
T-01	429.66	1.999E-04	0.13
IRD WS #2	431.06	2.006E-04	0.15
T-01	434.32	2.023E-04	0.12
IRD WS #2	440.19	2.056E-04	0.15
T-01	440.29	2.053E-04	0.12
T-01	444.93	2.077E-04	0.12
T-01	449.93	2.102E-04	0.12
IRD WS #2	450.10	2.108E-04	0.15
T-01	455.05	2.129E-04	0.12
T-01	459.76	2.152E-04	0.12
T-01	464.56	2.177E-04	0.12
T-01	467.82	2.193E-04	0.12
T-01	471.14	2.209E-04	0.12
T-01	475.33	2.230E-04	0.12
T-01	479.31	2.250E-04	0.12
T-01	484.24	2.275E-04	0.12
T-01	487.77	2.292E-04	0.12
T-01	491.37	2.310E-04	0.12
T-01	495.33	2.329E-04	0.12
T-01	500.59	2.355E-04	0.12
T-01	505.98	2.381E-04	0.12
T-01	509.52	2.400E-04	0.12
T-01	510.17	2.402E-04	0.13
T-01	515.43	2.428E-04	0.12
T-01	519.45	2.447E-04	0.12
T-01	530.51	2.498E-04	0.14
T-01	538.76	2.541E-04	0.12
T-01	543.40	2.564E-04	0.12
T-01	548.84	2.590E-04	0.12
T-01	554.31	2.617E-04	0.12
T-01	560.03	2.645E-04	0.12
T-01	564.79	2.668E-04	0.12
T-01	568.97	2.687E-04	0.12

T-01	574.76	2.716E-04	0.12
T-01	580.34	2.743E-04	0.12
T-01	585.33	2.766E-04	0.12
T-01	592.66	2.801E-04	0.12
T-01	593.17	2.803E-04	0.12
T-01	597.87	2.826E-04	0.12
T-01	597.87	2.826E-04	0.12
T-01	604.28	2.857E-04	0.12
T-01	609.63	2.882E-04	0.12
T-01	635.42	3.009E-04	0.30
T-01	640.30	3.027E-04	0.24
T-01	643.32	3.042E-04	0.14
T-01	645.67	3.053E-04	0.15
T-01	650.30	3.075E-04	0.22
T-01	655.27	3.102E-04	0.25
T-01	660.62	3.127E-04	0.17
T-01	665.16	3.151E-04	0.56
T-01	665.16	3.139E-04	0.41
T-01	668.28	3.165E-04	0.53
T-01	692.28	3.276E-04	0.12
T-01	696.75	3.298E-04	0.12
T-01	700.68	3.315E-04	0.29
T-01	701.90	3.323E-04	0.12
T-01	705.20	3.338E-04	0.19
T-01	705.65	3.340E-04	0.19
T-01	706.01	3.342E-04	0.12
T-01	710.28	3.362E-04	0.22
T-01	710.64	3.363E-04	0.14
T-01	710.80	3.365E-04	0.12
T-01	715.12	3.386E-04	0.16
T-01	715.40	3.387E-04	0.12
T-01	716.26	3.391E-04	0.12
T-01	719.33	3.406E-04	0.18
T-01	720.07	3.406E-04	0.26
T-01	721.71	3.416E-04	0.12
T-01	721.96	3.416E-04	0.24
T-01	725.66	3.435E-04	0.18
T-01	726.13	3.436E-04	0.12
T-01	730.38	3.456E-04	0.17
T-01	731.22	3.461E-04	0.12
T-01	735.43	3.481E-04	0.14
T-01	736.30	3.485E-04	0.12
T-01	740.32	3.504E-04	0.13
T-01	741.36	3.510E-04	0.12

T-01	746.08	3.531E-04	0.13
T-01	746.76	3.534E-04	0.12
T-01	750.72	3.551E-04	0.12
T-01	750.78	3.553E-04	0.13
T-01	751.13	3.555E-04	0.12
T-01	755.32	3.573E-04	0.12
T-01	756.84	3.580E-04	0.12
T-01	761.78	3.603E-04	0.12
T-01	761.86	3.605E-04	0.12
T-01	765.40	3.621E-04	0.12
T-01	765.40	3.622E-04	0.12
T-01	769.80	3.640E-04	0.12
T-01	774.63	3.663E-04	0.12
T-01	780.29	3.690E-04	0.12
T-01	785.25	3.714E-04	0.12
T-01	790.28	3.737E-04	0.12
T-01	794.98	3.759E-04	0.12
T-01	799.74	3.782E-04	0.12
T-01	805.36	3.808E-04	0.12
T-01	810.65	3.833E-04	0.12
T-01	815.19	3.854E-04	0.12
T-01	820.19	3.879E-04	0.12
T-01	820.61	3.880E-04	0.12
T-01	825.26	3.904E-04	0.12
T-01	829.52	3.923E-04	0.12
T-01	835.58	3.952E-04	0.12
T-01	840.40	3.974E-04	0.12
T-01	845.72	4.000E-04	0.12
T-01	850.66	4.021E-04	0.12
T-01	855.20	4.044E-04	0.12
T-01	860.71	4.070E-04	0.12
T-01	865.36	4.093E-04	0.12
T-01	870.05	4.113E-04	0.12
T-01	875.28	4.139E-04	0.12
T-01	880.09	4.161E-04	0.12
T-01	885.44	4.186E-04	0.12
T-01	889.87	4.207E-04	0.12
T-01	895.33	4.234E-04	0.12
T-01	899.86	4.255E-04	0.12
T-01	904.95	4.279E-04	0.12
T-01	910.10	4.303E-04	0.12

3.7 Uncertainty analysis for the Radiance Responsivity of GLAMR Si

Table 3.6 Uncertainty budget for absolute spectral radiance responsivity of GLAMR Si

	Relative Standard Uncertainty [%]	
Uncertainty Component	**347 nm to 400 nm and 400 nm to 450 nm from IRD WS #2**	**380 nm to 910 nm from T-01**
Reference detector Irrad. Cal.[1]	0.19 and 0.12	0.09
Measurement % St Dev[2]	0.02	0.05
Reference Detector Distance	0.02	0.01
Geometry Alignment	0.05	0.05
Amplifier Gain	0.05	0.05
Reference Detector Aperture Area	0.02	0.02
Sphere Aperture Area	0.03	0.03
Wavelength[3]	0.02	0.01
Total k = 1 % Uncertainty	**0.21 and 0.15**	**0.13**

Note 1: For the IRD WS #2 range the two different values correspond to the irradiance calibration from scaling the power responsivity (300 nm to 400 nm) and directly from T-01 (400 nm to 450 nm).
Note 2: This is the average measurement percent standard deviation across the entire range. Value for individual wavelengths are provided in the calibration file.
Note 3: Wavelength uncertainty was noticeably higher in the intracavity doubled LBO-OPO range from 540 nm to 610 nm and a value of 0.03 was used for the individual points in that range.
Note 4: This is not the full calibration uncertainty budget. The uncertainty budget, Table 3.4, does not include environmental effects on both the reference detector and the GLAMR radiometer. No evaluations of instrument performance characteristics such as temperature dependence, response linearity or temporal stability were performed. For estimates in the interpolated uncertainty, see the reference.[8]

4. General Information

It should be noted that the reported results were derived from using the dial gain value on the provided pre-amplifiers (i.e. 1 x 10^7 V/A) to give the radiance responsivity in [A/(W/cm^2/sr)]. This assumes that the transimpedance pre-amplifier for each DUT has been calibrated and the dial gain values have high accuracy (to say 0.05 % or better). If this is not the case, we need either to obtain the gain correction factors for those amplifiers or can only report the calibration for each device as a whole system (i.e. detector plus amplifier) in units of [V/(W/cm^2/sr)] for radiance.

Information was recorded in the SIRCUS Vis #20 laboratory notebook, pp.105-113 and pp 123-121.

The calibration measurements were performed by Brian Alberding and John Woodward. The data analysis and report writing was performed by Brian Alberding.

This calibration required 12 days of laboratory work (including setup, troubleshooting, and data collection) on SIRCUS and 7 days of data reduction, analysis, and reporting.

Significant experimental notes:

1. On Sept. 5, 2019, there was a problem communicating with the XY stage. After re-establishing communication and homing the stage the center XY positions significantly changed. New XY maps were completed for T-01 and GLAMR Si and new center positions were noted. Comparing the signal-to-monitor ratio with the previous day's results at a similar wavelength (~ 0.4 nm different) showed that the results were less than 0.1% different at the new XY positions. The calibration therefore proceeded from that point.
2. The radiance responsivity of GLAMR Si was measured in similar wavelength ranges from 380 nm to 450 nm using both the SHG of the Mai Tai laser emitted from the Inspire HF 100 and the SHG of the LBO-OPO signal. It should be noted that the two lasers gave significantly different results for the radiance responsivity of GLAMR Si versus T-01 in this range. The results from the Mai Tai SHG were lower and increasingly deviated as the wavelength was reduced towards 380 nm. The agreement was good at 450 nm to 0.009% but was 1.8 % different at 380 nm. It is possible the increased bandwidth of the Mai Tai laser (resulting from the shorter pulse width) could have some effect in this range where the Si photodiode response curve is not as linear. Therefore, the calibration versus T-01 used the results from the LBO-OPO signal SHG for the wavelength range down to 380 nm. For the calibration versus IRD WS #2 only the Mai Tai SHG from the Inspire HF 100 was used.
3. It should be noted that in the range 690 nm to 750 nm, the radiance responsivity of GLAMR Si when using the Mai Tai laser agreed within 0.025 % with the result when using the conventional Ti:Sapphire and Dye CW SIRCUS lasers (interpolated to common wavelength). Additionally, the measurement percent standard deviation when using the Mai Tai laser was significantly lower compared to the conventional SIRCUS lasers likely due to reduced speckle resulting from the larger bandwidth.

Information about data files:

1. Full data files for the radiance responsivity of GLAMR Si are located on Elwood under:

   \\cfs2e.nist.gov\685\internal\G04\Sircus\SIRCUS\Calibrations\SIRCUS Calibrations\FY 2019 Calibrations\GLAMR\GLAMR Si

   Data file for the radiance responsivity of GLAMR Si: "GLAMR Si Calibration Sept 2019_combined T-01 and IRDWS#2 Data.xlsx"

2. Full data files for the irradiance calibration of IRD WS #2 are located on Elwood under the same directory:

\\cfs2e.nist.gov\685\internal\G04\Sircus\SIRCUS\Calibrations\SIRCUS Calibrations\FY 2019 Calibrations\GLAMR\GLAMR Si

Data file for the absolute irradiance responsivity of IRD WS #2: "Irradiance Responsivity Analysis IRDWS#2 from T-01.xlsx"

The files located in these directories are meant for internal NIST use only. Please do not distribute without authorization.

References

1. Brown, S. W., Eppeldauer, G. P. & Lykke, K. R. Facility for spectral irradiance and radiance responsivity calibrations using uniform sources. *Appl. Opt., AO* **45**, 8218–8237 (2006).
2. Woodward, J. T. *et al.* Invited Article: Advances in tunable laser-based radiometric calibration applications at the National Institute of Standards and Technology, USA. *Review of Scientific Instruments* **89**, 091301 (2018).
3. Shaw, P.-S. Report of Calibration: Spectral Power Responsivity based on Absolute Cryogenic Radiometer for Si photodiodes SN IRD WS #1, IRD WS #2, UVG #16, and UVG #24. (2017).
4. Houston, J. M. & Rice, J. P. NIST reference cryogenic radiometer designed for versatile performance. *Metrologia* **43**, S31 (2006).
5. Alberding, B. G. & Woodward, J. T. Report of Test for the Absolute Spectral Irradiance Responsivity of the Silicon Trap Detector T-01 from T-06. (2018).
6. Shaw, P.-S. Report of Calibration for SIRCUS Si Trap Detectors T06 and T04 from 475 nm to 1000 nm. (2016).
7. Shaw, P.-S. Report of Calibration for SIRCUS Trap Detectors T06 and T04 from 364 nm to 470 nm. (2017).
8. Gardner, J. L. Uncertainties in Interpolated Spectral Data. *J. Res. Natl. Inst. Stand. Technol.* **108**, 69–78 (2003).

Distribution Restrictions: None

Tabulated calibration data files were provided along with this report.
Filename: "GLAMR Si Calibration Sept 2019_Data Delivered to NASA.xlsx"

Prepared by:

Brian G. Alberding
Remote Sensing Group
Sensor Science Division
Physical Measurement Laboratory
(301) 975-4664

Approved by:

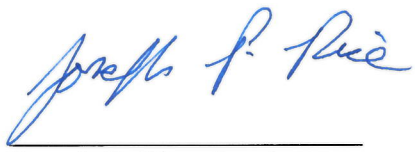

Joseph P. Rice, Leader
Remote Sensing Group
Sensor Science Division
Physical Measurement Laboratory
(301) 975-2133